Results in Physics 61 (2024) 107768

Contents lists available at ScienceDirect

Results in Physics

journal homepage: www.elsevier.com/locate/rinp

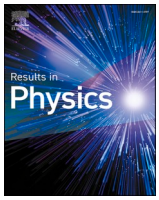

Magnetic and electric effects in magnetorheological suspensions based on silicone oil and polypyrrole nanotubes decorated with magnetite nanoparticles

Eugen Mircea Anitas [a,b], Andrei Munteanu [c], Michal Sedlacik [c,d,*,1], Ioan Bica [e], Lenka Munteanu [c], Jaroslav Stejskal [c]

[a] Horia Hulubei National Institute for R&D in Physics and Nuclear Engineering, Reactorului 30, RO-077125 Măgurele, Romania
[b] Joint Institute for Nuclear Research, Joliot Curie 6, 141980 Dubna, Moscow Region, Russia[2]
[c] Centre of Polymer Systems, Tomas Bata University in Zlín, Tr. T. Bati 5678, 76001 Zlín, Czech Republic
[d] Department of Production Engineering, Faculty of Technology, Tomas Bata University in Zlín, Vavreckova 275, 760 01 Zlín, Czech Republic
[e] West University of Timișoara, 4 V. Pârvan Ave., Timișoara 300223, Timiș County, Romania

ARTICLE INFO

Keywords:
Magnetorheological suspensions
Polypyrrole nanotubes
Magnetite nanoparticles
Relative dielectric permittivity
Dielectric loss factor
Active magnetic composites

ABSTRACT

In this work, two magnetorheological suspensions composed of polypyrrole nanorods decorated with magnetite nanoparticles and suspended in silicone oil were studied as electrical devices. The electrical devices (EDs) were fabricated in a unique cell using nanotubes with different magnetic and electric properties which can be tailored during synthesis. The electrical effects of the suspensions were studied under static electric and magnetic fields and were superimposed on a medium-frequency electric field. The electrical resistance Rp and the quality factor Qp at the terminals of EDs were extracted and analysed. Additionally, the equivalent electrical capacitances Cp were obtained through a well-established theory and then compared for each ED. Through the electrical and magnetic dipolar approximation model, it was illustrated that the electrical effect induced in a suspension can be three times higher depending on the amount of the magnetite. Thus, by tuning the synthesis parameters, it is possible to obtain EDs with well-defined and unique properties.

Introduction

Magnetorheological suspensions (MRSs) are colloidal intelligent materials consisting of magnetic microparticles which are dispersed in a non-magnetic carrier [1–4]. Under the influence of an external magnetic field, a magnetic phase is formed containing column-like aggregates which are oriented along the magnetic field lines [5,6]. In turn, this leads to a fast and reversible change of the material's mechanical and electrical properties, including magnetorheological [7,8], magneto-resistive [9] or magneto-dielectric (*MDE*) behaviour [10,11].

Numerous applications in various fields take advantage of the mentioned effects. The magnetorheological effect is mainly used in shock absorbers and mechanical vibrations [12–16], or in magnetically controllable clutches [17,18]. The MDE effect is a phenomenon in which the electrical capacitance or the relative dielectric permittivity are changed in the presence of a magnetic field. Well-known materials with good MDE properties are MRSs based on silicone oil (SO) and carbonyl iron (CI) microparticles [9] or MRSs absorbed by cotton fabrics [10], for which the relative dielectric permittivity and the dielectric loss factor can be tuned by an external magnetic field.

Several types of magnetic particles are generally used for applications. However, when mixed in a solution such magnetic particles tend to sediment due to the high density mismatch [19]. A good solution would be to use rod or tube-like particles [20]. Their high free volume leads to high entropic repulsions which improves the stability of the solution. For tube-like magnetic particles especially, the literature is extremely limited [21]. For that reason, tube-like particles were selected. However, as mentioned above, good electric properties are also

* Corresponding author at: Centre of Polymer Systems, Tomas Bata University in Zlín, Tr. T. Bati 5678, 76001 Zlín, Czech Republic.
E-mail addresses: eanitasro@gmail.com (E.M. Anitas), munteanu@utb.cz (A. Munteanu), msedlacik@utb.cz (M. Sedlacik), ioan.bica@e-uvt.ro (I. Bica), strouhalova@utb.cz (L. Munteanu), stejskal@utb.cz (J. Stejskal).
[1] ORCID: 0000-0003-3918-5084.
[2] International Intergovernmental Organization.

https://doi.org/10.1016/j.rinp.2024.107768
Received 23 April 2024; Accepted 15 May 2024
Available online 18 May 2024
2211-3797/© 2024 The Author(s). Published by Elsevier B.V. This is an open access article under the CC BY-NC license (http://creativecommons.org/licenses/by-nc/4.0/).

needed. Thus in this work, magnetic and conductive nanotubes are investigated as MDEs.

Another benefit of polypyrrole is its use in medical and environmental applications [22]. Environmentally friendly and low-cost MRSs have already been investigated. As an example, magnetically active membranes, consisting of honey, carbonyl iron, and silver microparticles, can be used for various biomedical applications since they allow a remote and magnetically induced release of the bioactive components [23]. For the case of electrical devices based on MRS with honey, the response occurs only upon the application of an external magnetic field. However, here by using PPMY particles, we expect that the response of the electrical device to occur both for external magnetic and electric fields something that other MDEs are lacking.

The aim of this work is twofold. Firstly, to show that it is possible for MRS based on SO and polypyrrole nanotubes decorated with magnetite nanoparticles to induce electro-magnetodielectric and electro-magnetoconductive effects, by using a medium-frequency electric field superimposed on static electric and magnetic fields. Secondly, to investigate which type of particles are responsible for these effects. To this aim, polypyrrole/magnetite (PPMY) nanoparticles were synthesised in two forms; PPMY6 and PPMY2.5 in accordance to the procedure described in Ref. [24]. Two MRSs, denoted MRS_1 and MRS_2 were prepared by using the same volume fractions of nanoparticles (PPYM6, and PPYM2.5, in the respective order), and SO. By using a measuring cell with a diameter of 20 mm and a height of 2 mm, two electrical devices (ED_1 and ED_2) are manufactured.

The electrical resistance R_p and the quality factor Q_p are measured at the terminals of the devices. Following, equivalent electrical capacitance C_p of each device is extracted from the obtained data. Further, C_p and R_p are used to determine the magneto-dielectric, magneto-electro-conductive (MCE), as well as electro-magnetodielectric and electro-magnetoconductive effects in the obtained suspensions. It is shown that the electro-magnetodielectric effects, and respectively the electro-magnetoconductive effects of MRS_1 are up to about three times higher as compared to MRS_2.

Experiment

Materials

The following materials were used for fabrication of MRSs; silicone oil (SO, MS 100 type produced by Silicone Commerciale SpA, Italy). The density of SO is $\rho_{SO} = 0.98$ g cm^{-3} and the kinematic viscosity is $\nu = 100$ cSt at 25 °C. The relative dielectric permittivity at the frequency $f = 100$ kHz and the same temperature is $\varepsilon_r = 2.8$. This type of SO can be used in a wide range of temperatures, from −55 °C up to 220 °C.

For the magnetic nanoparticles, a two-step synthesis was performed to obtain two kinds of nanotubes. The codenames of PPMY6 and PPMY2.5 were selected to emphasize the molar ratio of $FeCl_3{\cdot}6H_2O$ over pyrrole which was used to make each type of nanotubes. A detailed description of the synthesis is provided in our previous work Ref. [24].

The morphology of the nanoparticles was studied by scanning electron microscope (SEM) NOVA NanoSEM 450 (FEI, The Netherlands) and shown in Fig. 1. As can be seen, the tube-like shape was confirmed for both types of particles and the higher molar ratio of $FeCl_3{\cdot}6H_2O$ resulted in increased amount of magnetite covering the polypyrrole tubes (Fig. 1a) [24]. Regarding the size of both particles, the tubes appear to be approximately around 1–3 μm in length and diameter in a nanometer range. In magnetorheological fluids based on iron oxide nanorods, the larger the size of the nanorods resulted in a higher performance of the fluids [25].

The PPMY6 and PPMY2.5 nanoparticles, having remanent electrical polarization, form millimetric-size agglomerates with different morphology and a high degree of polydispersity, as shown in Fig. 2. In order to decrease the polydispersity degree, the agglomerates have been partially redispersed using a friction bowl with pestle, for about 15 min per sample.

The obtained particles P_1 and P_2 (Fig. 3a and 3b) have smaller sizes: the average diameter of P_1 is 12.55 μm and a standard deviation of 4.37 μm, and the average diameter of P_2 is 13.60 μm and a standard deviation of 4.14 μm, obtained by a fit with a lognormal distribution, as shown in Fig. 3c and 3d. By measuring the volumes and masses of $_{P1}$ and P_2, the densities $\rho_1 = 0.32$ g cm^{-3}, and $\rho_2 = 0.27$ g cm^{-3} respectively were extracted. The suspensions MRS_1 and MRS_2 were prepared by manual mixing of 1.5 cm^3 of SO and 1.5 cm^3 of P_1, and respectively P_2 microparticles, for about 10 min, in a 25 mL Berzelius glass.

The magnetization curves of the PPMY6 and PPMY2.5 nanoparticles have been obtained by a vibrating-sample magnetometer (VSM, Model 7407, USA) with the intensity of the magnetic field ranging from –796 to + 796 kA m^{-1} at room temperature. The results are shown in Fig. 4. As can be seen in Fig. 4a, PPMY6 show superior magnetization M_{SP}, exceeding 61 A m^2 kg^{-1}, in comparison to their counterpart which

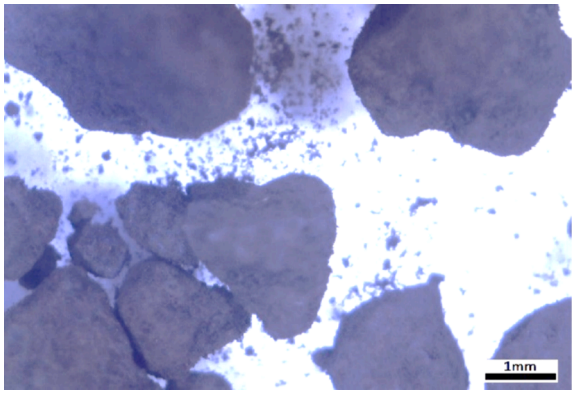

Fig. 2. The morphology of PPMY6 microparticles, obtained using a digital microscope. PPMY2.5 have a similar morphology.

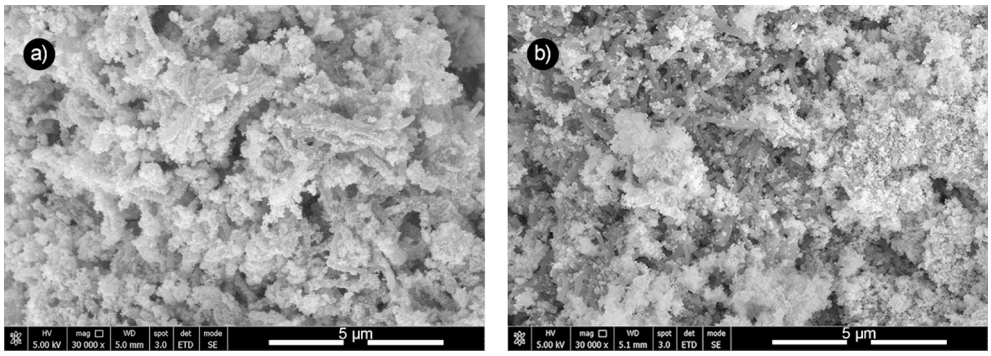

Fig. 1. The morphology of PPMY6 (a) and PPMY2.5 (b) evaluated by SEM.

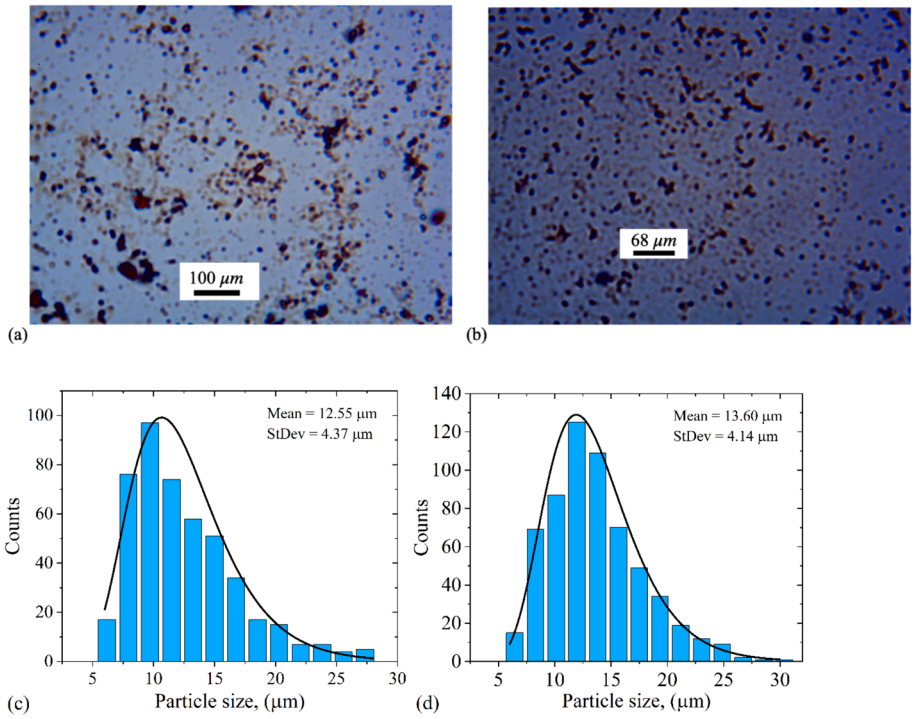

Fig. 3. Microparticles P_1 (a), and P_2 (b) visualized in transmission mode, by using OPTIKA microscope (made in Italy). The corresponding histograms of the equivalent diameters (blue bars) and the fit with a lognormal distribution function (black curve) for P_1 (c) and P_2 (d). (For interpretation of the references to colour in this figure legend, the reader is referred to the web version of this article.)

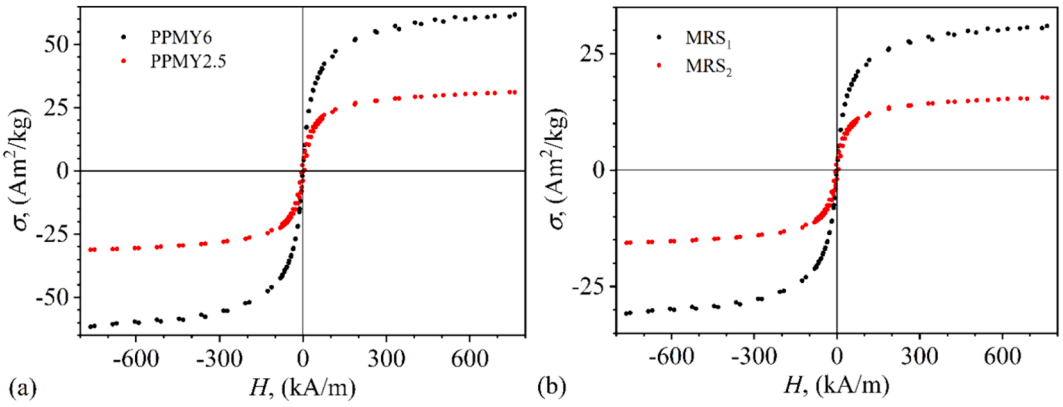

Fig. 4. The relative magnetization σ function of the intensity H of the magnetic field, for: a) particles PPMY6 and PPMY2.5; b) suspensions MRS_1 and MRS_2.

peaked at 31 A m^2 kg^{-1}. This indicates that especially PPMY6 particles are promising also for magnetorheological suspensions [24].

It is known that between the saturation magnetization M_{SP} of the particles and the saturation magnetization M_{MRS} of the suspensions, the following relationship holds: $\mu_0 M_{MRS} = \Phi_P \mu_0 M_{SP}$, [21], where μ_0 is the magnetic constant of the vacuum and Φ_P is the volume fraction of the particles. Since the volume fractions of particles P_1 and P_2 in their respective suspensions are 50 %, then by using the above relation together with the magnetization curves of the particles form Fig. 4a, one obtains in Fig. 4b the magnetization curves of MRS_1 and MRS_2. Note that when compared to the pure particles, it is apparent that in suspension form, the overall magnetization is significantly lower, due to decreased concentration of the magnetic nanoparticles, which are responsible for the magnetic response.

Fabrication of electrical devices

The materials used for the manufacture of the devices are:

- A copper foil with electroconductive adhesive (FCua) in the form of a roll (Fig. 5a), was purchased from Fruugo (UK). The length of the copper foil is 20 m, the width is 20 mm and thickness is 0.05 mm. The adhesive side is covered with a paper layer with a thickness of 0.5 mm.
- A surgical tape (ST), Durapore 3 M type, was obtained from Help Net (Fig. 5b, pos. 1) in the form of a roll. The length of the tape is 9.5 m, the width is 50 mm and the thickness is 0.2 mm. The outer side of ST is non-adhesive (Fig. 5b, pos. 1), while the inner side is adhesive (Fig. 5b, pos. 2).
- A crystal protection film (F), was purchased from Office Direct (Romania), in A4 format. The thickness of the foil is 0.12 mm.

Fig. 5. (a) Copper foil (pos. 1). Paper band on the side with electroconductive adhesive. (b) Surgical tape roll (pos. 1). The adhesive side of the tape (pos. 2). (c) Natural rubber pad.

- A self-adhesive pad (Ba), purchased from Carboy with a diameter of 40 mm and thickness of 2 mm (Fig. 5c). The pad is made from natural rubber and can support a weight of up to 700 N.

The EDs were manufactured according to the following steps:

1. Two pieces with dimensions 45 mm × 40 mm were cut from the ST band and the F coil. The adhesive side of ST was placed on the foil F by pressing.
2. The copper foil was placed on the non-adhesive side of the assembly made during step 1 by pressing until the surface area of ST was covered. As a result, the components of the measuring cell MC (Fig. 6a) were completed.
3. A hole with a diameter of 20 mm was made with a steel drill in the pad from Fig. 5(c). This part was placed with the adhesive side on the copper side of the assembly obtained during step 2 (Fig. 6b). As such, the second component of the measuring cell MC (Fig. 6b) is made.
4. The suspensions were then poured on the copper side, as shown in Fig. 7a. Following, the electrical device ED_1 with MRS_1, and the device ED_2 with MRS_2 were completed by electrically insulating the copper sides through the ST using heating. Fig. 7b show the final configuration of the obtained ED.

Experimental setup

The overall configuration of the experimental installation is shown in Fig. 8 (pos 6). The setup was used to study the magnetic suspensions in a medium-frequency electric field superimposed on a static magnetic field and uniform mechanical tension forces. The installation consists of an electromagnet, a direct current source (DCS), RXN-3020D type from HAOXIN (China), an RLC bridge Br, E720 type (Belarus), a gaussmeter Gs, DX-102 type from Dexing Magnets (China), a hall probe h, and a force application unit for the deformation of the device. The displacement unit is made of non-magnetic elements, and it consists of a shaft passing through the magnetic pole of the electromagnet and is mechanically coupled with a disk and a plate. The mass marked with a value of 800 g (Fig. 8) on the plate, is a lead disk. The ED and the probe h of the gaussmeter are fixed between the poles of the electromagnet utilizing a non-magnetic disk.

The working frequency f of the Br bridge is 10 kHz. The static magnetic field has magnetic flux density values B with a maximum of 420 mT, adjustable in steps of 30 mT. At the beginning, and during the measurements, the values of B were set within the limits of $\pm$ 2 %. The intensity E inside the EDs can be tuned in steps of 2 $kV_{dc}\ m^{-1}$ up to a maximum value of 20 $kV_{dc}\ m^{-1}$ by adjusting the voltage on the bridge.

Using the Br bridge, the parallel electrical resistance R_p and the quality factor Q_p of EDs are measured during the application of the magnetic field or the intensity of a static electric field. During the measurements, the impedance at the terminals of the RLC meter is fixed at 100 kΩ.

Experimental results, theoretical model and discussions

The effect of magnetic field $B \neq 0, E = 0$

The EDs are inserted one by one between the magnetic poles of the electromagnet. The resistance R_p and the quality factor Q_p of EDs are measured for magnetic flux density in the range $0 \leq B\ (mT) \leq 420$, periodically increased by steps of 30 mT in the absence of the static electric field. The recorded values are shown in Fig. 9.

Let us consider that nanoparticles P_1 and P_2 are monodisperse-like and uniformly distributed in the SO matrix (Fig. 10a). In the presence of a magnetic field, they become magnetic dipoles oriented along the magnetic field lines in the form of parallel and equidistant chains (Fig. 10b). Then, two identical and neighbouring magnetic dipoles form an electrical microcapacitor electrically connected in parallel with an electrical microresistor.

Through the values of R_p and Q_p, the equivalent electrical capacitance C_p is calculated using the following well-known formula:

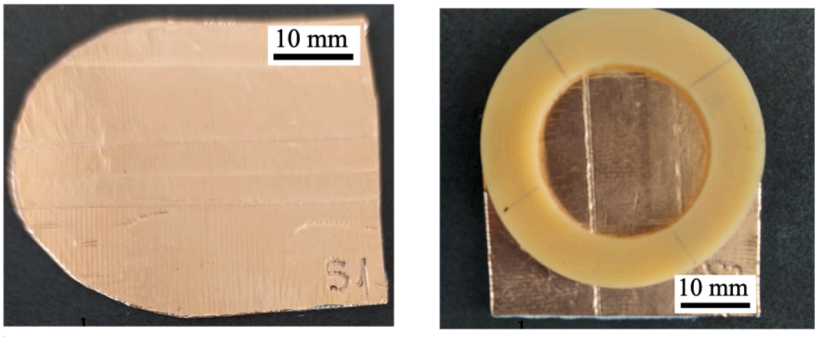

(a) (b)

Fig. 6. The components of the measuring cell MC. (a) Copper foil. (b) Natural rubber ring on top of the copper foil.

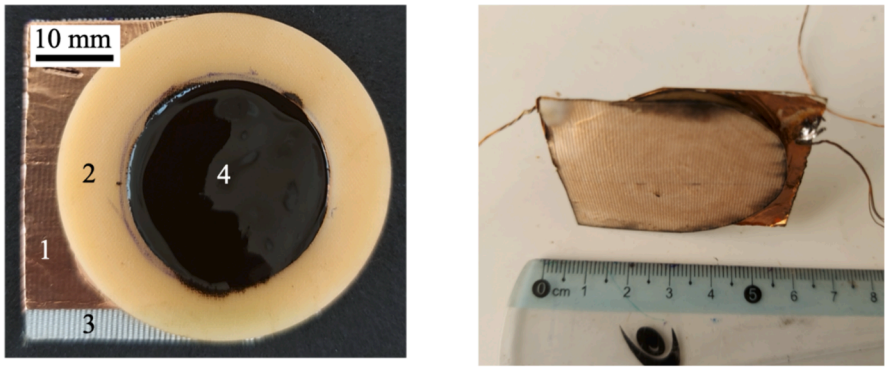

Fig. 7. (a) Subassembly with MRSs. (b) The end configuration of ED. 1 – copper foil, 2 – natural rubber ring with a diameter of 20 mm and thickness of 2 mm, 3 – ST band with non-adhesive surface, 4 – MRSs.

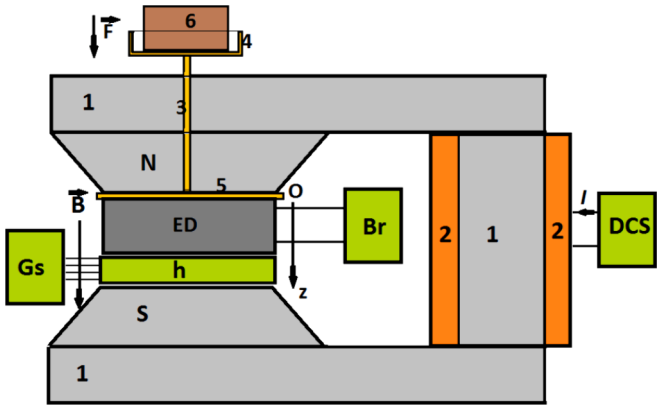

Fig. 8. Experimental setup (overall configuration): 1 – magnetic core, 2 – coil, 3 – non-magnetic spindle, 4 – non-magnetic plate, 5 – non-magnetic disk, 6 – non-magnetic marked mass, N and S – magnetic poles, ED – electrical device, Br – RLC bridge, Gs – gaussmeter, h – hall probe, DCS – continuous current source, Oz – coordinate axis, $\boldsymbol{B}$ – magnetic flux density vector, $\boldsymbol{F}$ – force vector, I – intensity of electric current.

$$C_{\mathrm{p}} = \frac{Q_{\mathrm{p}}}{2\pi f R_{\mathrm{p}}}, \tag{1}$$

Using the parameters mentioned in the experimental setup the above-mentioned formula can be rewritten:

$$C_{\mathrm{p}}(pF) \simeq \frac{16 Q_{\mathrm{p}}}{R_{\mathrm{p}}(\mathrm{M\Omega})}, \tag{2}$$

By using the variations $R_{\mathrm{p}} = R_{\mathrm{p}}\,(B)_{\mathrm{ED}}$ from Fig. 9a, and $Q_{\mathrm{p}} = Q_{\mathrm{p}}\,(B)_{\mathrm{ED}}$ from Fig. 9b, the variation of the capacitance can be deducted with the magnetic flux density, i.e. $C_{\mathrm{p}} = C_{\mathrm{p}}\,(B)_{\mathrm{ED}}$, as shown in Fig. 11a. The results in Figs. 9a and 11a suggest that EDs are real capacitors, whose equivalent electrical scheme consists of a resistor and a capacitor connected in parallel. In addition, R_{p} and Q_{p} decreases, and respectively increases with B, leading to an increase of the electrical conductivity.

Using the volume fractions of the magnetizable nanoparticles (representing the percentage of magnetizable particles in the MRS), from Ref. [26] it can be shown that the expressions for C_{p} and R_{p} can be written as:

$$C_p = \epsilon_0 \epsilon'_{MRS} \frac{S}{h_0}\left(1 - \frac{2.25\Phi S B^2}{\mu_0 k d}\right), \tag{3}$$

and

$$R_p = \frac{h_0}{S\sigma_0}\left(1 - \frac{2.25\Phi S B^2}{\mu_0 k d}\right), \tag{4}$$

respectively. Here, ϵ_0 is the vacuum dielectric constant, ϵ'_{MRS} the relative

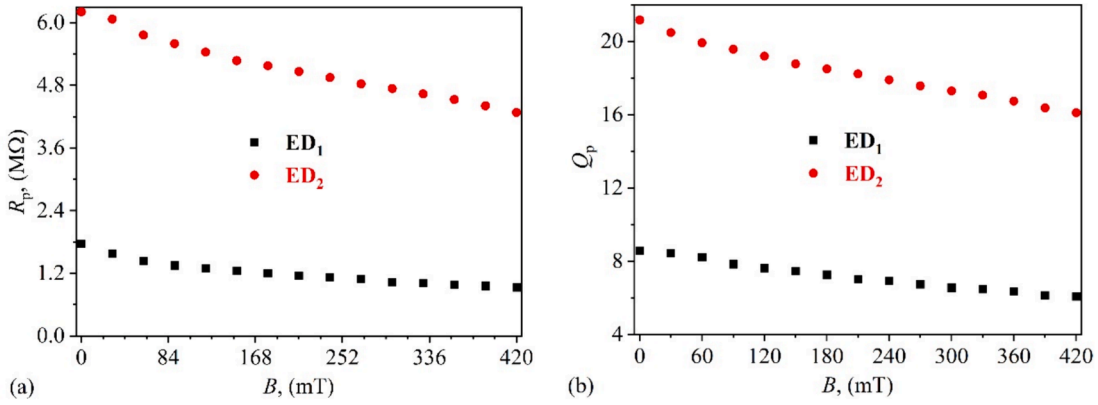

Fig. 9. Variation of the electrical resistance R_{p} (a) and of the quality factor Q_{p} (b) with the magnetic flux density B for ED_1 (black colour) and ED_2 (red colour). (For interpretation of the references to colour in this figure legend, the reader is referred to the web version of this article.)

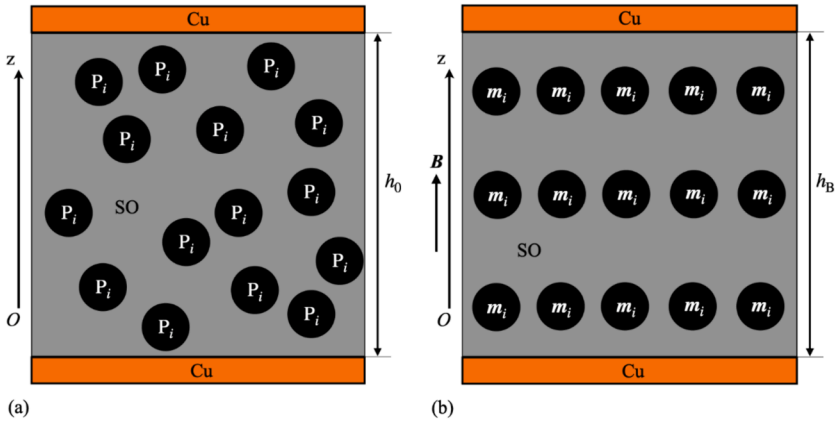

Fig. 10. Distribution of particles P_i (i = 1,2) in silicone oil (model) in the absence of a magnetic field (a), and respectively in the presence of a magnetic field (b). Here, $\boldsymbol{B}$ is the magnetic field density vector, $\boldsymbol{m}_i$ is the magnetic moment vector of particle P_i (i = 1, 2), Oz is the coordinate axis, h_0 and h_B are the distances between the copper plates (Cu) in the presence, and respectively in the absence of the magnetic field.

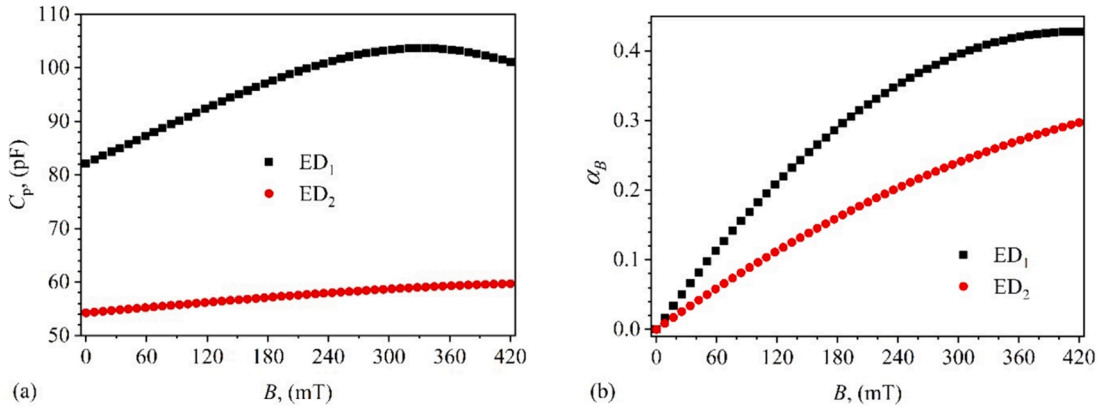

Fig. 11. Variation of the electrical capacitance C_p (a) and of the dimensionless quantity α_B (b) with the magnetic flux density B for ED_1 (black colour) and ED_2 (red colour). (For interpretation of the references to colour in this figure legend, the reader is referred to the web version of this article.)

dielectric permittivity of the suspensions, S represents the common surface area between the copper foil and MRS, h_0 refers to the thickness of MRS, Φ the volume fraction of nanoparticles inside MRS, μ_0 stands for the vacuum magnetic constant, k the deformability constant of the magnetic dipoles chain, d refers to the equivalent diameter of the magnetic dipoles, and equal to that of particles, and σ_0 is the electrical conductivity of MRS in the absence of the magnetic field.

Equations (3) and (4) show that the values of C_p and R_p are highly dependent on the magnetic flux density, in agreement with the experimental data from Fig. 9a and 11a. However, for the same values of the nanoparticles volume fractions, and for the same values of B, the values of R_p (Fig. 9a), and respectively of C_p (Fig. 11a) are different. According to the model given by Eqs. (3) and (4), the observed effect is due to the values of average diameters of the particles from MRS, and due to the values of the deformability constants of the magnetic dipole chains. In particular, an increase of either the average diameter or of the deformability constant leads to a less pronounced decrease of C_p and R_p with B.

To quantify the contribution induced by the diameters of magnetic dipoles and by the deformability constant of the chains they form, we introduce the magneto-deformation effect:

$$\alpha_B \equiv \frac{2.25\Phi S B^2}{\mu_0 k d}, \tag{5}$$

which describes the ratio between the deformation magnetic force of the magnetic dipole chains and the resistance force opposed by these chains. Therefore, by using Eqs. (4) and (5), α_B can be rewritten as:

$$\alpha_B = 1 - \frac{R_p}{R_{p0}}, \tag{6}$$

where $R_{p0} \equiv \frac{h_0}{S\sigma_0}$ is the resistance in the absence of the magnetic field.

By introducing in Eq. (6) the variation of resistance with magnetic flux density from Fig. 9a, variation of α_B with magnetic flux density is obtained, i.e. $\alpha_B = \alpha_B(B)$, as shown in Fig. 11b. The results show that α_B for P_1 particles is significantly higher when compared to P_2 particles. In particular, for $B \geq 300$ mT, α_B is about two times larger for P_1 microparticles, in agreement with the model of the magnetic dipole approximation and confirmed by the results obtained in [23,26,27].

The quantification of the type of nanoparticles on the behaviour of the capacitance and resistance is addressed by using the *MDE* and *MCE* effects, defined by:

$$MDE(\%) \equiv \left(\frac{C_p}{C_{p0}} - 1\right) \times 100, \tag{7}$$

and respectively by:

$$MCE(\%) \equiv \left(\frac{R_{p0}}{R_p} - 1\right) \times 100. \tag{8}$$

Thus, using the data from the capacitance and resistance from Fig. 9a, and 11a respectively, from the Eqs. (7) and (8), the variation of *MDE* and *MCE* are obtained, as shown in Fig. 12a, and respectively 12b. The

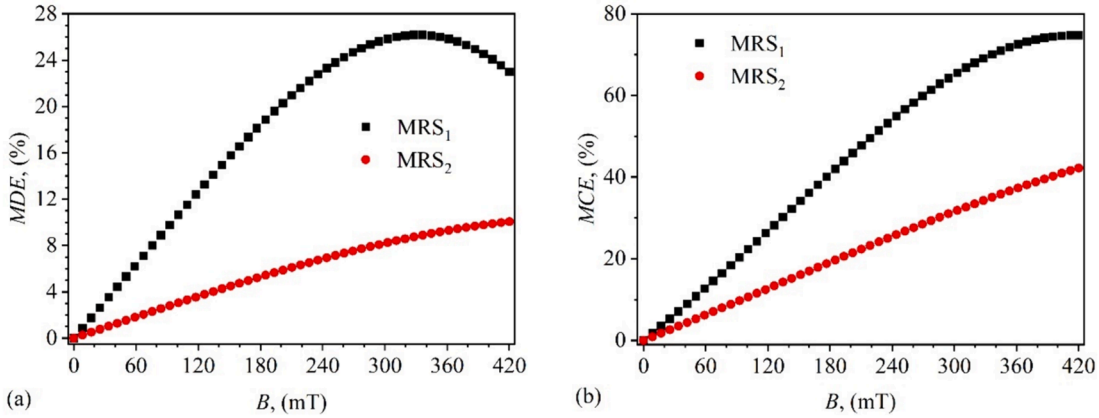

Fig. 12. Variation of the *MDE* (a) and of the *MCE* (b) with the magnetic flux density B for ED_1 (black colour) and ED_2 (red colour). (For interpretation of the references to colour in this figure legend, the reader is referred to the web version of this article.)

results indicate that the type of particles used can significantly influence the MRSs *MDE* and *MCE*. In particular, for $B > 0$, the contribution of the P_1 nanoparticles is higher if compared to P_2 nanoparticles, for both *MDE* and *MCE*. This is due to the different structure and stoichiometric composition of P_1 and P_2.

The observed effects resulted from the magnetization of the two types of particles (see Fig. 4b), as they are responsible for the occurrence of different magnetic forces, and thus for different magneto-deformations of the magnetic dipole chains in MRSs [24,27]. As a result of the interaction between the magnetic dipole chains, for P_1 particles, the resistance (Fig. 9a) and capacitance (Fig. 11a) induce the maximum at $B \simeq 340$ mT in *MDE* (Fig. 12a) and *MCE* (Fig. 12b). Through their proximity and the agglomeration process, the number of columns with electric microcapacitors and microresistors decreases. This leads to a decrease of resistance R_p and capacitance C_p, therefore changing the behaviour of *MDE* and *MCE* for MRS_1 sample.

The effect of electric field $\boldsymbol{B} = 0, \boldsymbol{E} \neq 0$

The quantities R_p and Q_p are measured as a function of the intensity E of a static electric field, and in the absence of magnetic field. Using the electric field, the samples were scanned from 0 to 20 kV m^{-1}, in intervals of 2 kV m^{-1}. The results are presented in Fig. 13a, and 13b respectively showing that EDs are equivalent, from an electrical point of view, to a resistor connected in parallel to a capacitor.

The electric field between the copper foils of EDs is uniformly distributed. As a result, the P_i, ($i = 1, 2$) particles obtain electrical charges q, thus becoming electrical dipoles. Within the volumes of MRSs, the quantity of charge can be expressed by [26]:

$$Q = \frac{6\Phi S q}{\pi d^2}. \tag{9}$$

Similarly to the magnetic dipoles, the electrical dipoles are oriented along the electric field lines, in the form of columns. This formation behaviour is illustrated in Fig. 14. We assume that these columns have equal lengths and are uniformly distributed in the MRS. In an electric field, the length h_0 of the columns becomes $h_E < h_0$ (as illustrated in Fig. 14).

By using the variations $R_p = R_p(B)$ and $Q_p = Q_p$ (B) from Fig. 9 in Eq. (2), the variation of capacitance $C_p = C_p(B)$ can be calculated as demonstrated in Fig. 15a. From the above assumptions and according to the model developed in Ref. [26], the length h_E can be calculated as:

$$h_E = h_0\left(1 - \frac{QE}{h_0 k_E}\right), \tag{10}$$

where k_E is the deformability constant of the electric dipole chains. Thus, by knowing h_E, we obtain the equivalent electrical capacitance of EDs in static magnetic field, as:

$$C_p = \frac{C_{p0}}{1 - \frac{QE}{h_E k_E}}, \tag{11}$$

where:

$$C_{p0} \equiv \frac{\epsilon_0 \epsilon'_{MRS} S}{h_0} \tag{12}$$

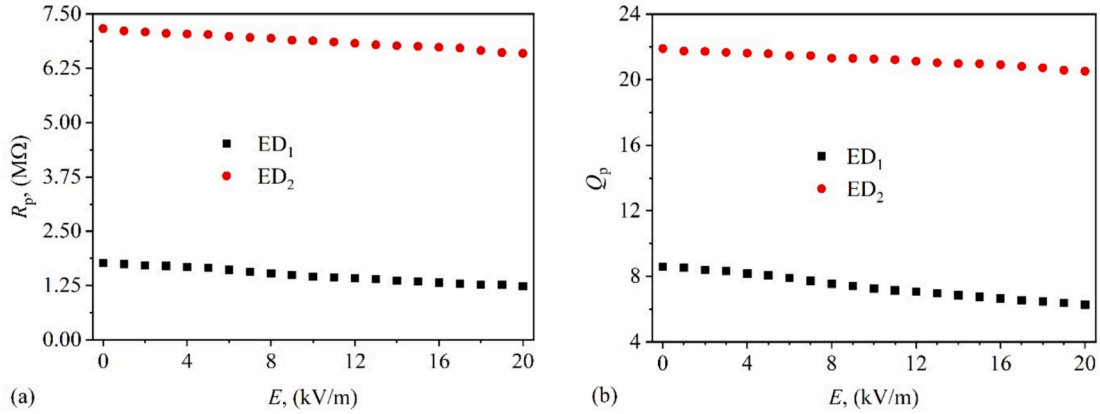

Fig. 13. Variation of the electrical resistance R_p (a) and of the quality factor Q_p (b) with the intensity E of a static electric field for ED_1 (black colour) and ED_2 (red colour). (For interpretation of the references to colour in this figure legend, the reader is referred to the web version of this article.)

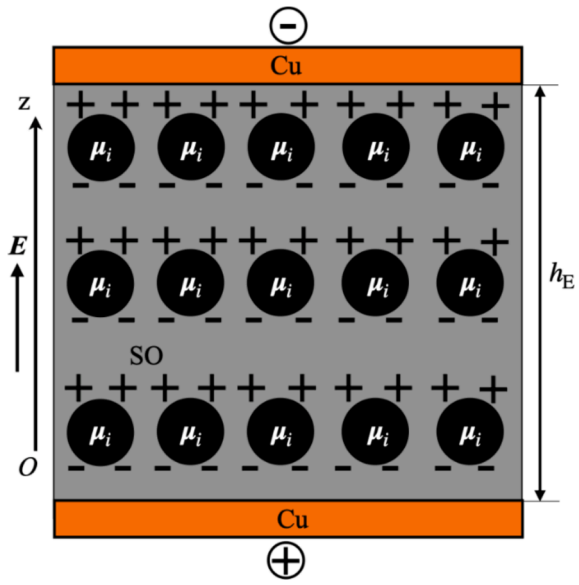

Fig. 14. Distribution of particles P_i (i = 1, 2) in silicone oil (model) in the presence of a static electric field. Here, E is the electric field intensity vector, $\boldsymbol{\mu}_1$ (i = 1, 2) is the electric moment, Oz is the coordinate axis, and h_E is the distances between the copper plates (Cu) in the presence, of the electric field. For the configuration without electric field, see Fig. 10a.

is the equivalent electrical capacitance of EDs in the absence of the electric field.

Similarly, the electrical resistance can be written as:

$$R_p = R_{p0}\left(1 - \frac{QE}{h_E k_E}\right), \tag{13}$$

where:

$$R_{p0} \equiv \frac{h_0}{\sigma_{MRS} S} \tag{14}$$

is the equivalent electrical resistance of EDs in the absence of electric field.

Equations (13) and (14) show that the values of the capacitance and resistance are greatly influenced by the values E of the intensity of the electric field, in agreement with experimental data from Figs. 9a and 11a. However, for the same volume fractions values of the particles, and for the same values of the intensity of the electric field, the values of C_p, and R_p are varied. According to the model given by Eqs. (13) and (14) the observed effects arise due to the values of the average diameters of the particles, as well as due to the deformability constants of the electrical dipole chains.

In order to quantify the contributions of these two factors, we introduce the electro-deformation effect:

$$\alpha_E \equiv \frac{QE}{h_E k_E}, \tag{15}$$

which describes the ratio between the electrical force of deformations of electrical dipole chains, and the resistance force opposed by the chains.

By combining Eqs. (13) and (15), one obtains α_E in the form:

$$\alpha_E \equiv 1 - \frac{R_p}{R_{p0}}. \tag{16}$$

Then, by using the variation of resistance from Fig. 11a in Eq. (16), the variation $\alpha_E = \alpha_E(E)$ can be obtained, as shown in Fig. 15b.

The results show that for $E > 0$, $\alpha_E(E)_{ED1} > \alpha_E(E)_{ED2}$. This effect arises due to the difference in the electrical polarization of particles P_1 and P_2, at a fixed value of intensity $E > 0$.

For the quantification of the contribution of the particles type to the capacitance and resistance, we introduce the relative contribution of the electric field, in the absence of the magnetic field, to the electrical capacitance (Λ_C) and to resistance (Λ_R), as:

$$\Lambda_C(\%) = \left(\frac{C_p}{C_{p0}} - 1\right) \times 100, \tag{17}$$

and respectively:

$$\Lambda_R(\%) = \left(\frac{R_{p0}}{R_p} - 1\right) \times 100. \tag{18}$$

Then, by using the variation of the capacitance (Fig. 11a) and of the resistance (Fig. 9a), the variations $\Lambda_C = \Lambda_C(E)$, and $\Lambda_R = \Lambda_R(E)$ are obtained as shown in Fig. 16a and 16b respectively. The results show that Λ_C and Λ_R have a quasi-linear increase with E, while $\Lambda_{C_{MRS1}} > \Lambda_{C_{MRS2}}$ and $\Lambda_{R_{MRS1}} > \Lambda_{R_{MRS2}}$ for $E > 0$. These effects can be correlated to the different values of the modulus of the electrical polarization vector, and the electrical conductivities of particles P_1 and P_2 [26] due to the accumulation of electrical charges in the volume of MRS and due to the electro and magneto-deformations of the column dipoles. In turn, this leads to an increase of the electrical conductivity and capacitance.

The combined effect of the electric and magnetic fields $\boldsymbol{B} \neq 0, \boldsymbol{E} \neq 0$

The EDs are introduced in a static electric field superimposed over a static magnetic field and an electric field of frequency $f = 10$ kHz with an effective value of $u = 1V_{ef}$. The intensity of the static electric field is

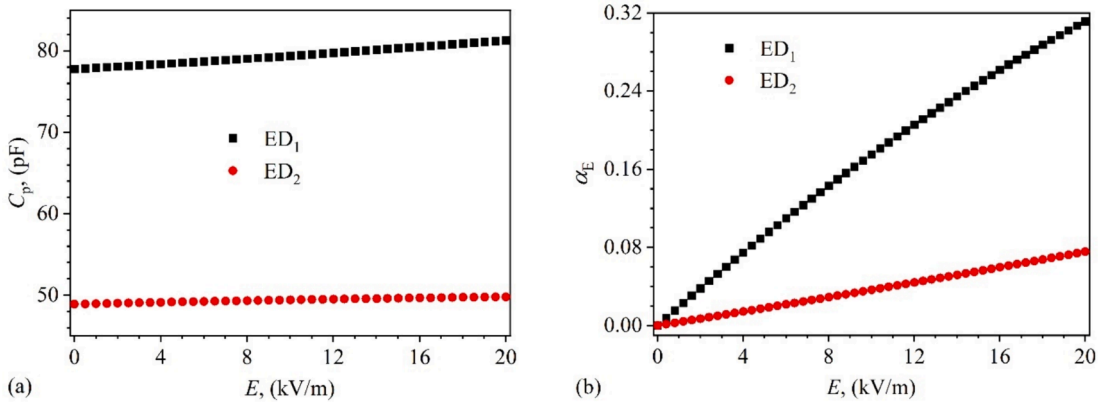

Fig. 15. Variation of the electrical capacitance C_p (a) and the quantity α_E (b) with the intensity E of a static electric field for ED_1 (black colour) and ED_2 (red colour). (For interpretation of the references to colour in this figure legend, the reader is referred to the web version of this article.)

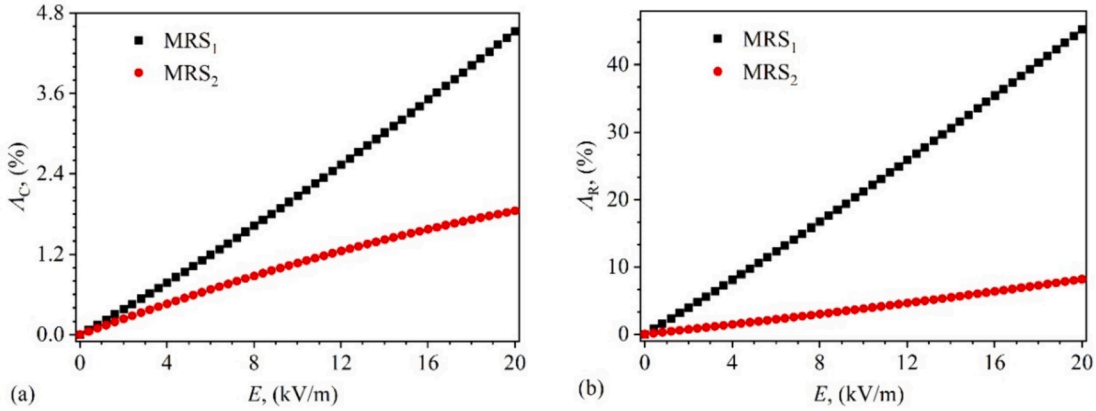

Fig. 16. Variation of Λ_C (a) and Λ_R (b) with the intensity E of a static electric field for MRS_1 (black colour) and MRS_2 (red colour). (For interpretation of the references to colour in this figure legend, the reader is referred to the web version of this article.)

steadily increased from 0 to 20kV m^{-1} in steps of 2 kV m^{-1}. The static magnetic field is also altered within the range of 0 and 0.4 T in steps of 100 mT. R_p and Q_p are measured during the application of the electric and magnetic fields. The obtained values for ED_1 and ED_2 are presented in Figs. 17 and 18, respectively. The results show that for both devices R_p (and Q_p) decrease with increasing values of the electric field in agreement with Eq. (13). When the electric field is fixed, R_p and Q_p decrease with increasing values of the magnetic field. Thus, R_p and Q_p are greatly influenced by the static electric and magnetic fields superimposed on a medium-frequency electric field.

Using the data from Figs. 17 and 18 in Eq. (2) the capacitances of ED_1 and ED_2 can be obtained, as shown in Fig. 19a, and b.

The results show that for fixed values of magnetic field, the capacitance has a quasi-linear increase with the electric field, in agreement with Eq. (11). Similarly, considering the fixed values of electric field, the capacitance increases significantly with increasing magnetic field, in agreement with Eq. (3). However, for fixed values of magnetic field the contribution of P_1 particles to the capacitance is two times larger when compared to P_2 particles. The effect is due to the high magnetic and electric polarization of P_1 particles compared to P_2 particles.

The quantification of the contribution of these fields, to the values of the relative dielectric permittivity of MRSs is examined by introducing the electro-magnetodielectric effect β_C, defined as:

$$\beta_C(\%) = \left(\frac{C_p(E)_B}{C_p(E)_{B=0}} - 1\right) \times 100, \tag{19}$$

where $C_p(E)_B$ is the capacitance when $E \neq 0$ and $B \neq 0$, and $C_p(E)_{B=0}$ is the capacitance when $E \neq 0$ and $B = 0$ T. By using the variation of the capacitance from Fig. 19, the variation of the electro-magnetodielectric effect can be evaluated, as shown in Fig. 20. The results show that for fixed values of field, the β_C increases for higher values of the magnetic field. Increasing both fields, leads to the agglomeration of dipole columns [26], which in turn results to a change of the shape of functions $\beta_C = \beta_C(E)$.

The quantification of the contribution of the static electric and magnetic fields superimposed on the medium-frequency electric field, to the electrical conductivities of MRSs is performed by introducing the electro-magnetoconductive quantity β_R, defined as:

$$\beta_R(\%) = \left(\frac{R_p(E)_{B=0}}{R_p(E)_B} - 1\right) \times 100, \tag{20}$$

where $R_p(E)_{B=0}$ is the resistance when $E \neq 0$ and $B = 0$ mT, and $R_p(E)_B$ is the resistance when $E \neq 0$ and $B \neq 0$. Thus, by using the variation of resistances form Figs. 17 and 18, it is possible to obtain the variation of the electro-magnetoconductive effects, as depicted in Fig. 21. The dependence of the electrical conductivity on the electric field superimposed on the magnetic is also clearly observed. Due to the interactions between column dipoles, the effect of dipole columns agglomeration is much more pronounced for MRS_1 as compared to MRS_2, for high values of B.

Conclusions

In this work, two suspensions with considerable magnetorheological properties are manufactured. Silicone oil was utilised as a liquid carrier

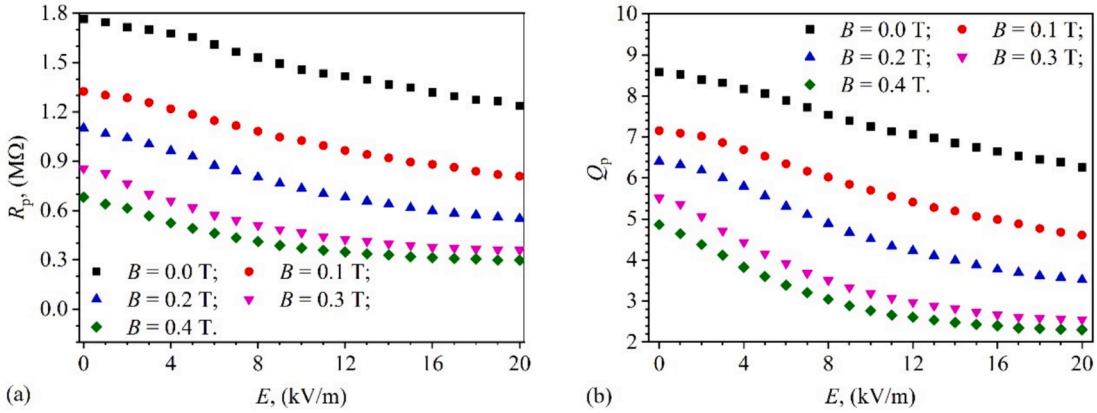

Fig. 17. Variation of the electrical resistance R_p (a) and of the quality factor Q_p (b) with the intensity E of a static electric field for ED_1, at fixed values of magnetic flux density B.

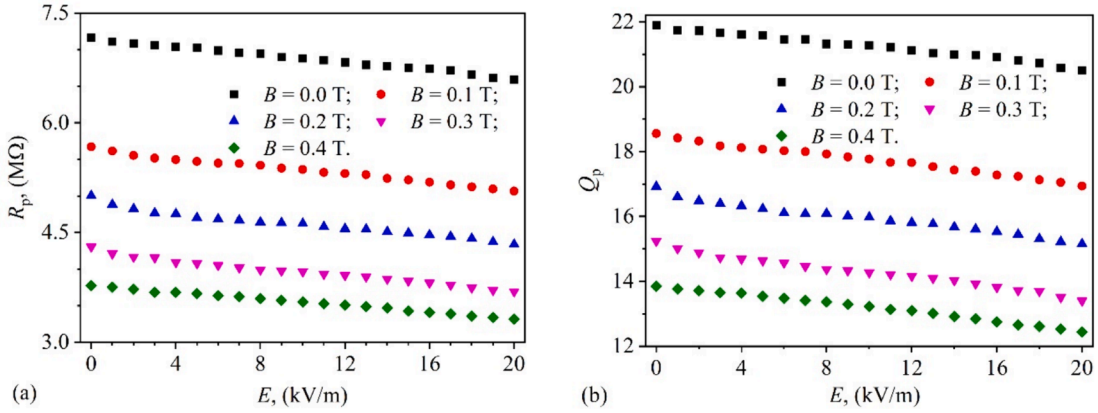

Fig. 18. Variation of the electrical resistance R_p (a) and of the quality factor Q_p (b) with the intensity E of a static electric field for ED_2, at fixed values of magnetic flux density B.

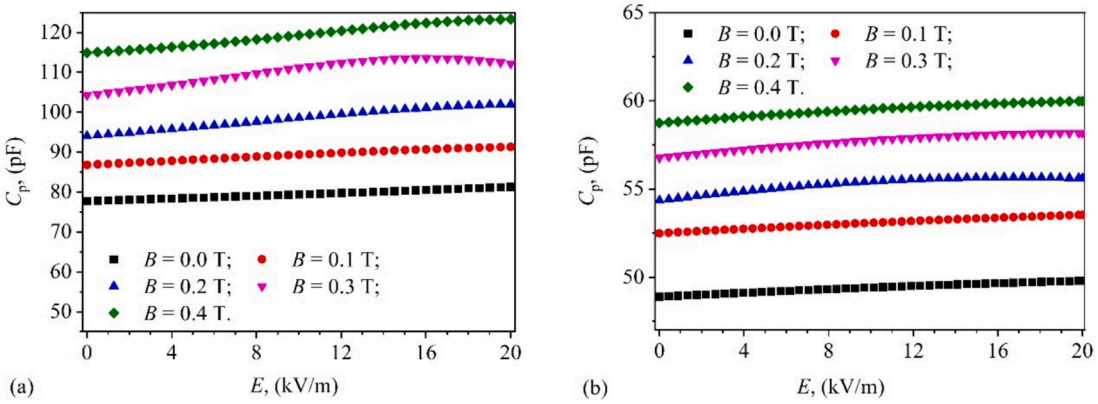

Fig. 19. Variation of the electrical capacitance C_p with the intensity E of a static electric field and at fixed values of magnetic flux density B, for ED_1 (a) and ED_2 (b).

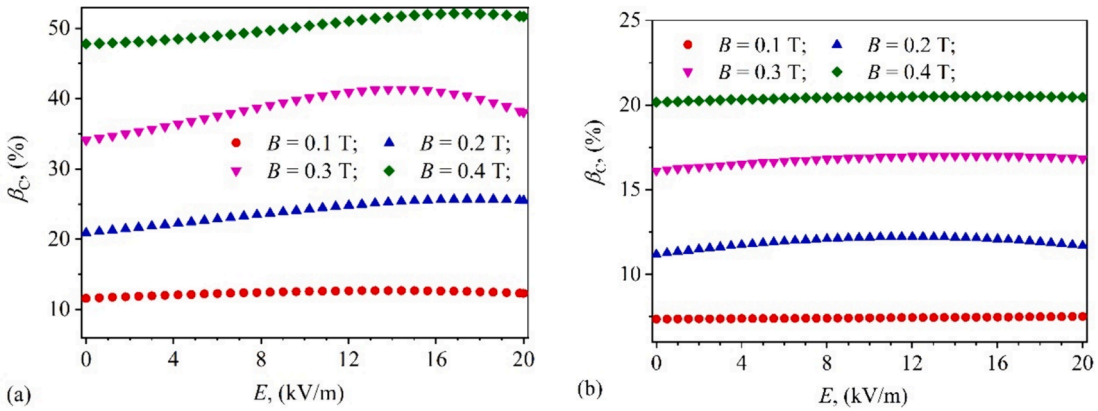

Fig. 20. Variation of the electro-magnetodielectric effect β_C with the intensity E of a static electric field and at fixed values of magnetic flux density B, for MRS_1 (a) and MRS_2 (b).

and two types of fillers (P_1 and P_2) as dispersed phase were compared. The fillers consist of polypyrrole nanotubes decorated with magnetite nanoparticles (PPYM6 and PPYM2.5). Each magnetorheological suspension contains the same volume fraction of PPYM6 and PPYM2.5 nanoparticles, and the same volume of silicone oil. Furthermore, the suspensions are used as dielectric materials for fabrication of electrical devices. An experimental setup is built to measure the electrical resistance and the quality factor at the terminals of the devices in the presence of static electric and magnetic fields superimposed on a medium-frequency electric field.

Based on the experimental results, the electrical capacitance of the capacitor is obtained. It is shown that the behaviour of both resistance and capacitance can be well described qualitatively by the models of electrical and magnetic dipolar approximations, and respectively by using the principle of effects superposition. An important feature is that in spite of the equal amounts of matrix and fillers, the induced electro-magnetodielectric effect (e.g. at $B = 0.4$ T and $0 \leq E(\mathrm{kV\,m^{-1}}) \leq 20$; Fig. 20), and the electro-magnetoconductive effect (e.g. at $B = 0.4$ T and $12 \leq E(\mathrm{kV\,m^{-1}}) \leq 20$; Fig. 21) is higher up to about three times for

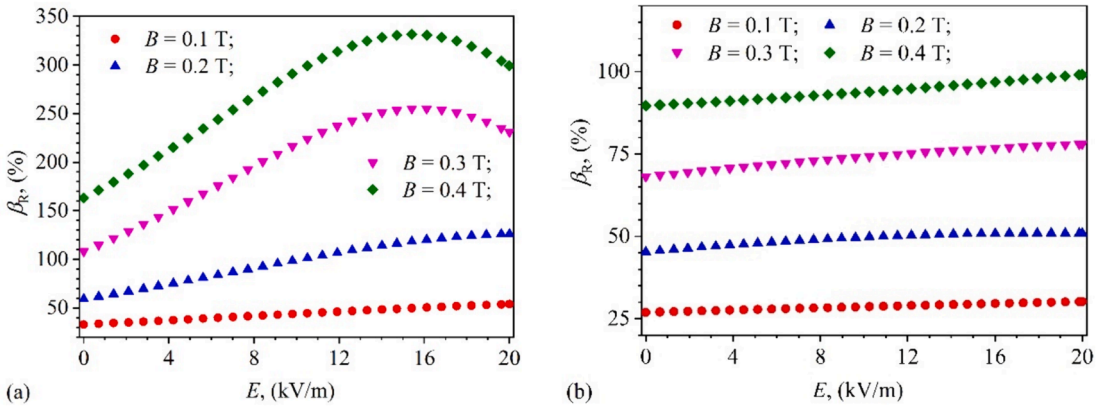

Fig. 21. Variation of the electro-magnetoconductive effect β_R with the intensity E of a static electric field and at fixed values of magnetic flux density B, for MRS_1 (a) and MRS_2 (b).

suspensions with P_1 particles.

These properties are important for the device manufacturing for monitoring electric and magnetic fields and respectively electromagnetic fields, as it is well-known that they contribute to pollution affecting life.

CRediT authorship contribution statement

Eugen Mircea Anitas: Investigation, Visualization, Writing – original draft. **Andrei Munteanu:** Investigation, Writing – original draft. **Michal Sedlacik:** Conceptualization, Funding acquisition, Supervision, Writing – review & editing. **Ioan Bica:** Conceptualization, Formal analysis, Investigation, Methodology. **Lenka Munteanu:** Investigation, Visualization, Writing – review & editing. **Jaroslav Stejskal:** Conceptualization, Methodology.

Declaration of competing interest

The authors declare the following financial interests/personal relationships which may be considered as potential competing interests: Michal Sedlacik reports financial support was provided by Czech Science Foundation. If there are other authors, they declare that they have no known competing financial interests or personal relationships that could have appeared to influence the work reported in this paper.

Data availability

Data will be made available on request.

Acknowledgements

The authors A.M., L.M., and M.S. wish to thank the Czech Science Foundation [23-07244S] for the financial support. This work and the project were realized with the financial support of the internal grant of the TBU in Zlín No. IGA/CPS/2024/008 funded from the resources of specific university research.

References

[1] S. Genc, Experimental studies on magnetorheological fluids, (2022).
[2] Bica I, Liu YD, Choi HJ. Physical characteristics of magnetorheological suspensions and their applications. J Ind Eng Chem 2013;19(2):394–406.
[3] Nika G, Vernescu B. Multiscale modeling of magnetorheological suspensions. Z Angew Math Phys 2020;71:1–19.
[4] Osial M, Pregowska A, Warczak M, Giersig M. Magnetorheological fluids: A concise review of composition, physicochemical properties, and models. J Intell Mater Syst Struct 2023;21.
[5] de Vicente J, Klingenberg DJ, Hidalgo-Alvarez R. Magnetorheological fluids: a review. Soft Matter 2011;7(8):3701–10.
[6] Jeong JY, Kim S, Baek E, You CY, Choi HJ. Suspension rheology of polyaniline coated manganese ferrite particles under electric/magnetic fields. Colloid Surf A-Physicochem Eng Asp 2023;656:130438.
[7] Pei P, Peng Y. The squeeze strengthening effect on the rheological and microstructured behaviors of magnetorheological fluids: A molecular dynamics study. Soft Matter 2021;17(1):184–200.
[8] Plachy T, Cvek M, Munster L, Hanulikova B, Suly P, Vesel A, et al. Enhanced magnetorheological effect of suspensions based on carbonyl iron particles coated with poly (amidoamine) dendrons. Rheol Acta 2021;60:263–76.
[9] Lu Q, Balasoiu M, Choi HJ, Anitas EM, Bica I, Cirigiu LME. Magneto-dielectric and viscoelastic characteristics of iron oxide microfiber-based magnetoreological suspension. J Ind Eng Chem 2022;112:58–66.
[10] Bica I, Anitas E. Magnetic flux density effect on electrical properties and viscoelastic state of magnetoactive tissues. Compos B Eng 2019;159:13–9.
[11] Bica I, Anitas E. Magnetodielectric effects in hybrid magnetorheological suspensions based on beekeeping products. J Ind Eng Chem 2019;77:385–92.
[12] Acharya S, Tak RSS, Singh SB, Kumar H, Characterization of magnetorheological brake utilizing synthesized and commercial fluids, Mater Today: Proc 2021:46; 9419-24.
[13] Bica I. Damper with magnetorheological suspension. J Magn Magn Mater 2002;241 (2–3):196–200.
[14] Deng Z, Wei X, Li X, Zhao S, Zhu S. Design and multi-objective optimization of magnetorheological damper considering vehicle riding comfort and operation stability. J Intell Mater Syst Struct 2022;33(9):1215–28.
[15] Yang J, Ning D, Sun S, Zheng J, Lu H, Nakano M, et al. A semi-active suspension using a magnetorheological damper with nonlinear negative-stiffness component. Mech Syst Sig Process 2021;147:107071.
[16] Tang X, Du H, Sun S, Ning D, Xing Z, Li W. Takagi-Sugeno fuzzy control for semi-active vehicle suspension with a magnetorheological damper and experimental validation. IEEE/ASME Trans Mechatron 2016;22(1):291–300.
[17] Shiao Y, Kantipudi MB. High torque density magnetorheological brake with multipole dual disc construction. Smart Mater Struct 2022;31(4):045022.
[18] Bica I. Magnetorheological suspension electromagnetic brake. J Magn Magn Mater 2004;270(3):321–6.
[19] Choi SB. Sedimentation stability of magnetorheological fluids: the state of the art and challenging issues. Micromachines 2022;13(11):1904.
[20] Bombard AJF, Goncalves FR, Morillas JR, de Vicente J. Magnetorheology of dimorphic magnetorheological fluids based on nanofibers. Smart Mater Struct 2014;23(12):125013.
[21] Ko SW, Yang MS, Choi HJ. Adsorption of polymer coated magnetite composite particles onto carbon nanotubes and their magnetorheology. Mater Lett 2009;63 (11):861–3.
[22] Stejskal J, Trchova M. Conducting polypyrrole nanotubes: a review. Chem Pap 2018;72(7):1563–95.
[23] Bica I, Iacobescu G-E. The influence of magnetic fields on the electrical conductivity of membranes based on cotton fabric, honey, and microparticles of carbonyl iron and silver. Materials 2023;16(5):1995.
[24] Stejskal J, Sapurina I, Vilcakova J, Plachy T, Sedlacik M, Bubulinca C, et al. Conducting and magnetic composites polypyrrole nanotubes/magnetite nanoparticles: Application in magnetorheology. ACS Appl Nano Mater 2021;4(2): 2247–56.
[25] Gwon H, Park S, Lu Q, Choi HJ, Lee S. Size effect of iron oxide nanorods with controlled aspect ratio on magneto-responsive behavior. J Ind Eng Chem 2023;124: 279–86.
[26] Bica I, Bălăşoiu M, Sfirloaga P. Effects of electric and magnetic fields on dielectric and elastic properties of membranes composed of cotton fabric and carbonyl iron microparticles. Results Phys 2022;35:105332.
[27] Melle S, Study of the dynamics in MR suspensions subject to external fields by means of optical techniques: aggregation processes, structure formation and temporal evolution, Madrid, 1995.